Preprint Title	Growth and Removal Behavior of Magnesium Oxide Microspheres towards Methyl Orange and Methylene Blue in Aqueous Solution
Authors	Saeed Ahmed, Jingsong Pan, Dianqing Li, Pinggui Tang, Xin Shu and Yongjun Feng
Publication Date	09 Jan 2020
Article Type	Full Research Paper
ORCID® iDs	Saeed Ahmed - https://orcid.org/0000-0002-9872-4474; Yongjun Feng - https://orcid.org/0000-0001-9254-6219

Growth and Removal Behavior of Magnesium Oxide Microspheres towards Methyl Orange and Methylene Blue in Aqueous Solution

Saeed Ahmed,[1] Jingsong Pan,[2] Dianqing Li,[1] Pinggui Tang,[1] Xin Shu,*[,1] Yongjun Feng*[,1, 3]

[1] State Key Laboratory of Chemical Resource Engineering, College of Chemistry, Beijing Engineering Center for Hierarchical Catalysts, Beijing University of Chemical Technology, No. 15 Beisanhuan East Road, Chaoyang District, Beijing 100029, China.

[2] Shandong Institute of Industry and Information Technology, No. 134, Jiefang Road, Jinan, Shandong Province, 250013, China

[3] Anqing Research Institute, Beijing University of Chemical Technology, No. 8 Huanhu West Road, High-Tech district, Anqing city, Anhui, 24600, China.

Corresponding author

*E-mail: shuxin@mail.buct.edu.cn (X. Shu),

*E-mail yjfeng@mail.buct.edu.cn, (Y.J. Feng) Fax: +86 10 6444 8071; Phone: +86 10 6444 8071

ABSTRACT

The adsorption of dyes from the industrial influent has attracted great interest to overcome water pollution. In this work, we carefully investigated the growth process of hierarchical MgO microspheres and the difference in the corresponding removal behavior towards two dyes: anionic methyl orange and cationic methylene blue. The MgO microspheres were formed by the self-assembly of thin nanosheets following the reaction time and exhibited the maximum removal capacities are 940.14 mg g^{-1} for methyl orange and 354.00 mg g^{-1} for methylene blue. The anionic methyl orange and cationic methylene blue adsorption follow the pseudo-second-order kinetic model, Freundlich isothermal model. The difference in the removal behavior towards two dyes is strongly related to the surface charge of MgO and the charge of pollutants. This work will benefit design and improvement in the removal performance of novel porous adsorbents.

Keywords: Magnesium oxide; Methyl orange; Methylene blue. Microsphere; Removal;

INTRODUCTION

Various kinds of colorful dyes have immensely enriched our lives as we image [1-2]. Yet, more and more residual dyes are directly discharged into the environment during the manufacturing and operation process [3], which are causing several adverse effects on the living system and even threatening human health [4-7]. Therefore, it is of great urgency and increasing interest to limit the discharge and reduce the concentration of the dyes in the environment [8-9].

Recently, the hierarchical three dimensional MgO microspheres have shown promising removal capacity of various dyes due to wide pore distribution, suitable pore size, and large surface area [10]. More recently, we established an ethylene glycol (EG) assisted room temperature method to produce the flower-like MgO microspheres with the excellent removal capacity for phosphate, for example, 574.71 mg g^{-1} [11]. Yet, the growth process of the MgO microsphere is still not clear. Besides, the surface charge is another important parameter to determine the removal performance related to target pollutants [12-15]. Till now, few reports have been published on the relationship between the surface charge on MgO and the removal capacity for a certain dye. Therefore, it remains a special interest to explore the formation process of the MgO microsphere in our previous work and the influence of MgO surface charge on the removal performance towards anionic and cationic dyes.

In this work, we carefully investigated the growth process of flower-like porous MgO microsphere following the reaction time and furthermore examined the removal performance of the obtained MgO microspheres towards two probe dyes: anionic methyl orange and cationic methylene blue as a function of MgO surface charge in the aqueous solution. Figure 1 shows the scheme of the possible growth mechanism of MgO microspheres and the removal process for dye-containing polluted water. The MgO microspheres are formed by the combination of nanosheets by electrostatic interaction between EG and Mg^{2+} in the synthesis system. This study provides an insight to choose suitable adsorption material based on the nature of the target pollutant.

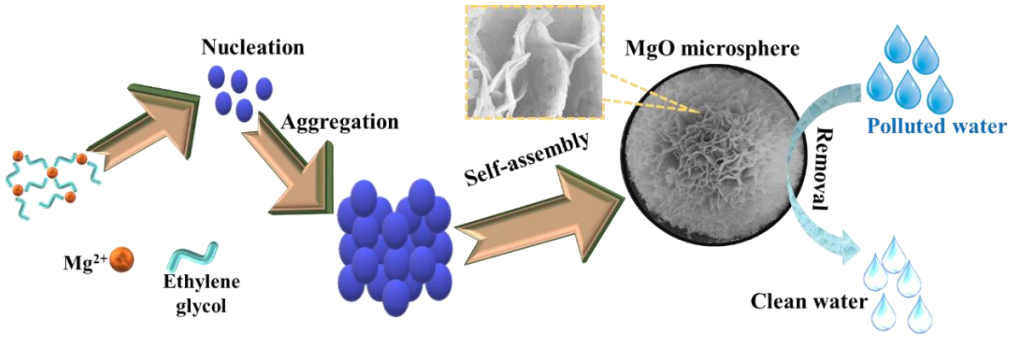

Figure 1 Growth scheme of hierarchical flower-like porous magnesium oxide microspheres for the adsorption of dyes.

MATERIALS AND METHOD

Chemicals

Methyl orange ($C_{14}H_{14}N_3NaO_3$), methylene blue ($C_{16}H_{18}ClN_3S$), anhydrous magnesium sulfate ($MgSO_4$), ethylene glycol ($C_2H_6O_2$, 98%), and ammonia solution (NH_3, 25-28 wt%) were analytical grade and used as provided by ALADDIN (Shanghai, China) without extra purification.

Synthesis of MgO microspheres

A series of hierarchical porous MgO microspheres were prepared in an EG assisted method as described in our previous work [10]. Briefly, 6.02 g (0.05 mol) $MgSO_4$ was added into 0.10 L water under stirring and then 31.04 g (0.50 mol) of EG was added into the $MgSO_4$ solution with the ratio of 10 between EG and Mg^{2+}. The Mg^{2+} ions were precipitated using 80 mL (0.80 mol) ammonia with a controlled addition rate using a peristaltic pump. The formed precipitates were collected after the desired time interval to monitor the microsphere precursor growth by washing with ethanol and water then drying for 12 h at 80 °C. The final MgO powder was calcined at 500 °C for 3 h with a rising rate of 1° per minute.

Characterization

X-ray diffraction patterns of precursor and MgO powder were carried out on powder X-ray diffractometer (Rigaku, Ultima III) in the range of 10-80°/2θ, and morphology was determined by scanning electron microscope (SEM, ZEIS SUPRA 5500). The pH values were monitored using Mettler Toledo FE20 pH meter with LE438 electrode combination with a resolution of 0.01. The dye concentration was quantitatively estimated using a UV-vis spectrophotometer (UV 2501 PC) at the corresponding wavelength of 464 nm and 664 nm for methyl orange and methylene blue, respectively.

Adsorption experiments

For the adsorption kinetic experiment, 10.0 mg MgO sample was dispersed into 100 mL (50 mg L^{-1}) methyl orange/methylene blue solution with different initial pH, after adjustment with 0.1 mol L^{-1} hydrochloric acid or sodium hydroxide, and placed into thermostat shaker with shaking speed of 180 rpm at 30 °C. The samples were collected after the desired time interval, and

separated by microfiltration membrane, while the remaining amount of methyl orange/methylene blue was quantitatively measured. The adsorption capacity with contact time *t* was calculated using equation 1. where q_t (mg g^{-1}) is the removal capacity with contact time *t*, and C_t (mg L^{-1}) is the dye concentration at contact time *t*;

$$q_t = (C_o - C_t)\, V/_m \quad (1)$$

For the adsorption isotherm experiment, 5.0 mg MgO was dispersed into the conical beakers containing 25 mL (30 - 300 mg L^{-1}) methyl orange and (10 - 150 mg L^{-1}) for methylene blue and placed into thermostat shaker for 8 h at 30 °C at the shaking speed of 180 rpm. After the equilibrium, the sample was collected, and separated by microfiltration membrane, while the remaining amount of methyl orange/methylene blue was measured spectrophotometrically. The equilibrium adsorption capacity of dyes at each concentration was calculated using equation 2;

$$q_e = (C_o - C_e)\, V/_m \quad (2)$$

For the zero-point charge determination, 20.0 mg MgO was dispersed into a conical beaker containing 25 mL water with different initial pH from 3-11 and placed into thermostat shaker for 12h to attain equilibrium. The equilibrium pH was measured while the change in pH was calculated using equation 3, where pH_i and pH_e are the initial and equilibrium pH of solutions respectively.

$$\Delta pH = pH_e - pH_i \quad (3)$$

RESULTS AND DISCUSSION

Morphology and structure

Figure 2 demonstrates the morphology of precursors collected at different reaction times and the X-ray diffraction patterns for the final precursor. Here, the lamellar sheets were observed at the beginning, for example, 5 min (Figure 2A) to 10 min (Figure 2B), and then these lamellar sheets are further arranged to form a flower-like bud (Figure 2C), which aggregates to form a hollow sphere with more aggregation ratio (Figure 2D) [16]. Finally, the petals are arranged regularly to build up a flower-like 3D microsphere (Figure 2E). This regular arrangement of sheets is related to the electrostatic interaction between EG and Mg^{2+} in the synthesis system[17]. Figure 2F shows the X-ray diffraction pattern for the final precursor, and matched well with the standard pattern for the magnesium hydroxide (PDF no. 86-0441). Eight diffraction peaks occur at 18.57°,

32.98°, 38.18°, 50.90°, 58.61°, 62.14°, 68.26°, and 72.12°/2θ, which individually correspond to the (001), (110), (101), (102), (110), (111), (103) and (201) for the magnesium hydroxide phase.

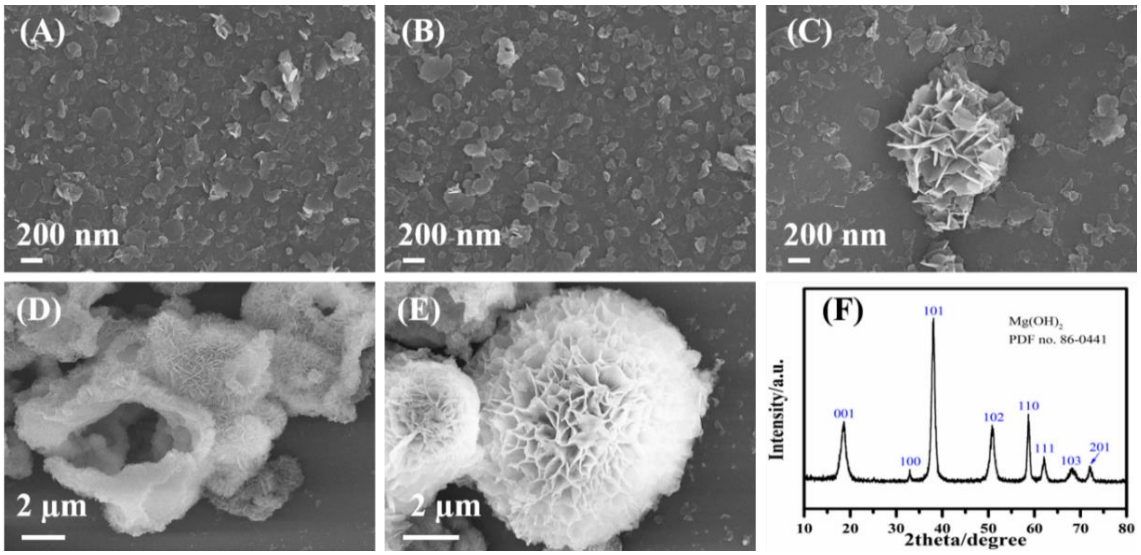

Figure 2 SEM images of MgO precursors collected at different reaction times: (A) 5 min, (B) 10 min, (C) 20 min, (D) 30 min, and (E) 40 min; and X-ray diffraction pattern of the final precursor at 40 minutes (F).

Figure 3 presents the X-ray diffraction pattern and morphology of the MgO sample, formed after calcination at 500 ºC under air atmosphere. The X-ray diffraction pattern for the MgO sample matches with the standard pattern for the cubic close-packed MgO phase (PDF no. 45-0946). Different five diffraction peaks at 37.35°, 43.33°, 62.48°, 74.62°, and 78.54°/2θ which correspond to the (111), (200), (220), (311), and (222) for the MgO phase. Figures 3B and 3C demonstrate the morphology of MgO, which is composed of lamellar sheets arranged orderly to form macroporous flower-like microspheres. These macropores may favor accelerating the adsorption rate, which is build up by the electrostatic interaction between EG and Mg^{2+} as reported in the literature for different metal oxides [18-20].

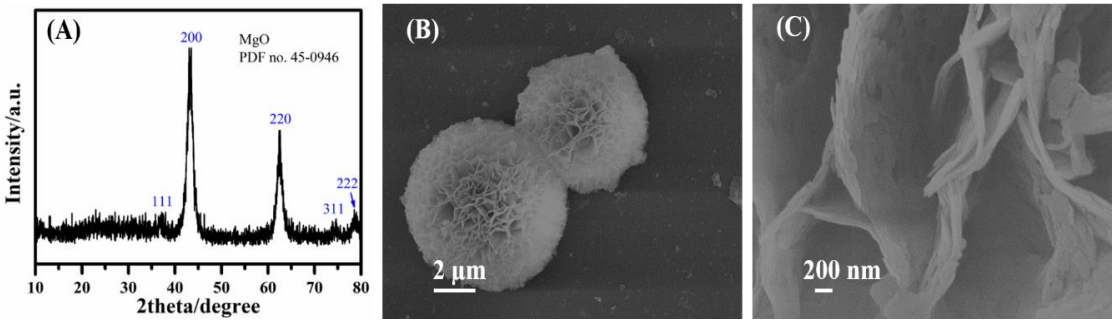

Figure 3 X-ray diffraction pattern (A) and SEM images for MgO with different magnifications (B, C).

Pore structure

Figure 4A presents the nitrogen N_2 isotherm assessed by the Brunauer-Emmett-Teller method. MgO exhibits the type II isotherm represents macropores with unhindered monolayer adsorption while an H3 hysteresis loop suggests the slit-like pores with boundless adsorption [21], and similar to the results observed from the SEM (Figure 3B). Figure 4B further demonstrates the pore size distribution in the range of ca. 1.5-137.0 nm. The prepared MgO microspheres exhibit the BET surface area of 75 m^2 g^{-1} with an average pore size of 28.7 nm and a pore area of 0.53 cm^3 g^{-1}. There are several macropores also present in flower-like MgO microsphere, which cannot be estimated based on the N_2 adsorption-desorption isotherm, and mercury intrusion method was used for macropores estimation. Figure 4C presents the variation of intrusion volume with pressure based on the mercury intrusion method. Figure 4D further demonstrates the macropore distribution present in the hierarchical flower-like MgO microspheres. There are several pores of different volumes beyond 1 µm range in the MgO microsphere as marked in Figure 4D, and these results also agree with the observed from the morphology. These results suggest that the pores of different size from nanometer (average pore size 28.7 nm) to the micrometer (average pore size 220.0 nm) present in the flower-like MgO microsphere, which may provide a pathway to approach the internal surface area of MgO based on nature of pollutant [22-24].

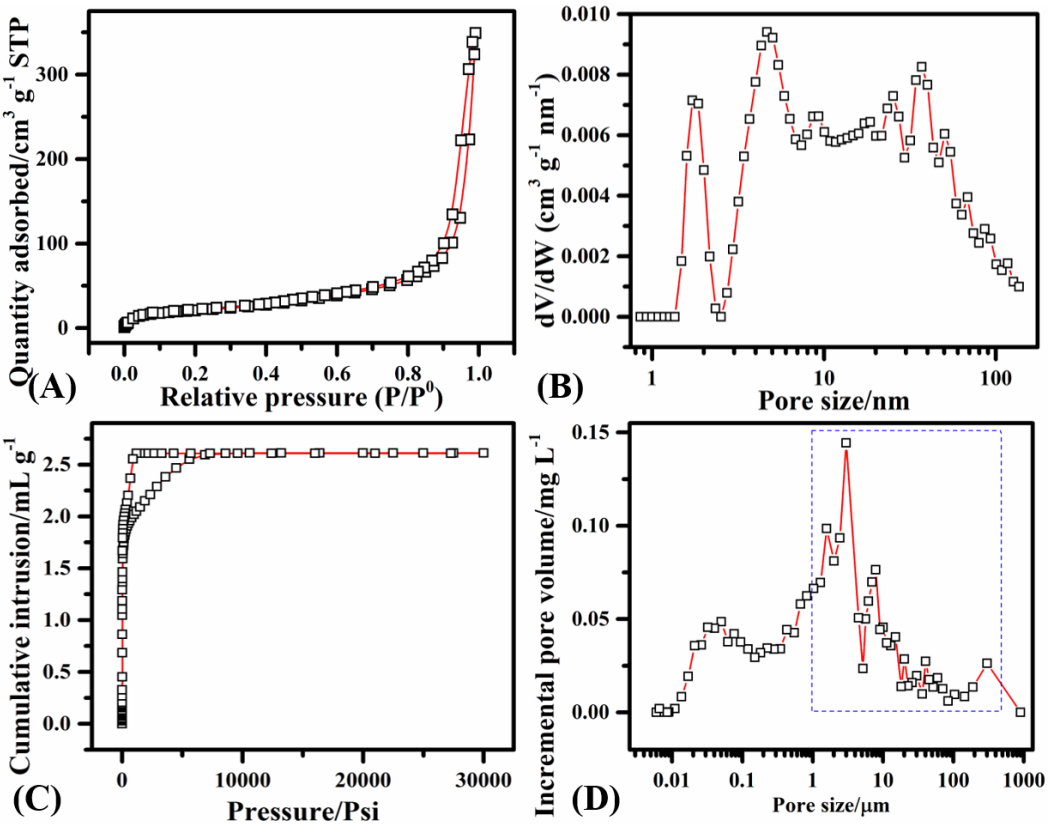

Figure 4 (A) Nitrogen adsorption-desorption isotherm (B) Pore size distribution (C) Cumulative intrusion volume (D) Macropore distribution for the hierarchical flower-like porous MgO microsphere.

Adsorption of methyl orange

The adsorption kinetics and isotherm experiments were conducted to evaluate the adsorption rate and removal capacity for methyl orange. Figure 5A displays the adsorption behavior of methyl orange under the different initial pH values of solution using hierarchical MgO microspheres. The MgO sample shows different removal capacities at the same equilibrium time of ca. 8 h for different initial pH values. The removal ability is reduced with the increase of the initial solution pH value under similar investigated conditions, which may be related to the different surface charges. Fig. 5B and 5C further show the linear fitting of pseudo-first-order and pseudo-second-order. The methyl orange adsorption follows the pseudo-second-order kinetic compared with the

first order based on the correlation coefficient values (Table 1), suggesting a mixed adsorption process under the investigated conditions.

Figure 5D shows the adsorption isotherm for methyl orange at neutral pH under the examined concentration range with the highest removal capacity of 940.14 mg g^{-1}. The attained isotherm data were linearly fitted for two well-known Langmuir and Freundlich models as shown in Fig. 5E and 5F. The adsorption behavior of methyl orange obeys the Freundlich isotherm model much better than the Langmuir isotherm model based on the correlation coefficient values in Table 2, suggesting the multilayer coverage of MgO by methyl orange. The separation parameter (R_L) [25] was calculated using equation 4, and the value of R_L between 0-1 also indicates the feasible methyl orange adsorption [26]. The maximum Langmuir adsorption capacity of methyl orange is 940.14 mg g^{-1}, which is much higher compared with recent adsorbent materials for methyl orange as listed in Table 3.

$$R_L = {}^{1}/_{1 + K_L C_o} \quad (4)$$

Table 1 Adsorption kinetic fitting parameters for methyl orange.

Initial pH	**$q_{e,exp}$/mg g^{-1}**	**Pseudo first order**			**Pseudo second order**		
		$q_{e,cal}$/mg g^{-1}	**k_1**	**R^2**	**$q_{e,cal}$/mg g^{-1}**	**k_2**	**R^2**
4	437.32	5.80	0.13	0.85	444.44	0.01	0.99
7	411.46	6.18	0.13	0.95	420.17	0.01	0.99
10	377.90	3.40	0.01	0.97	362.89	0.01	0.99

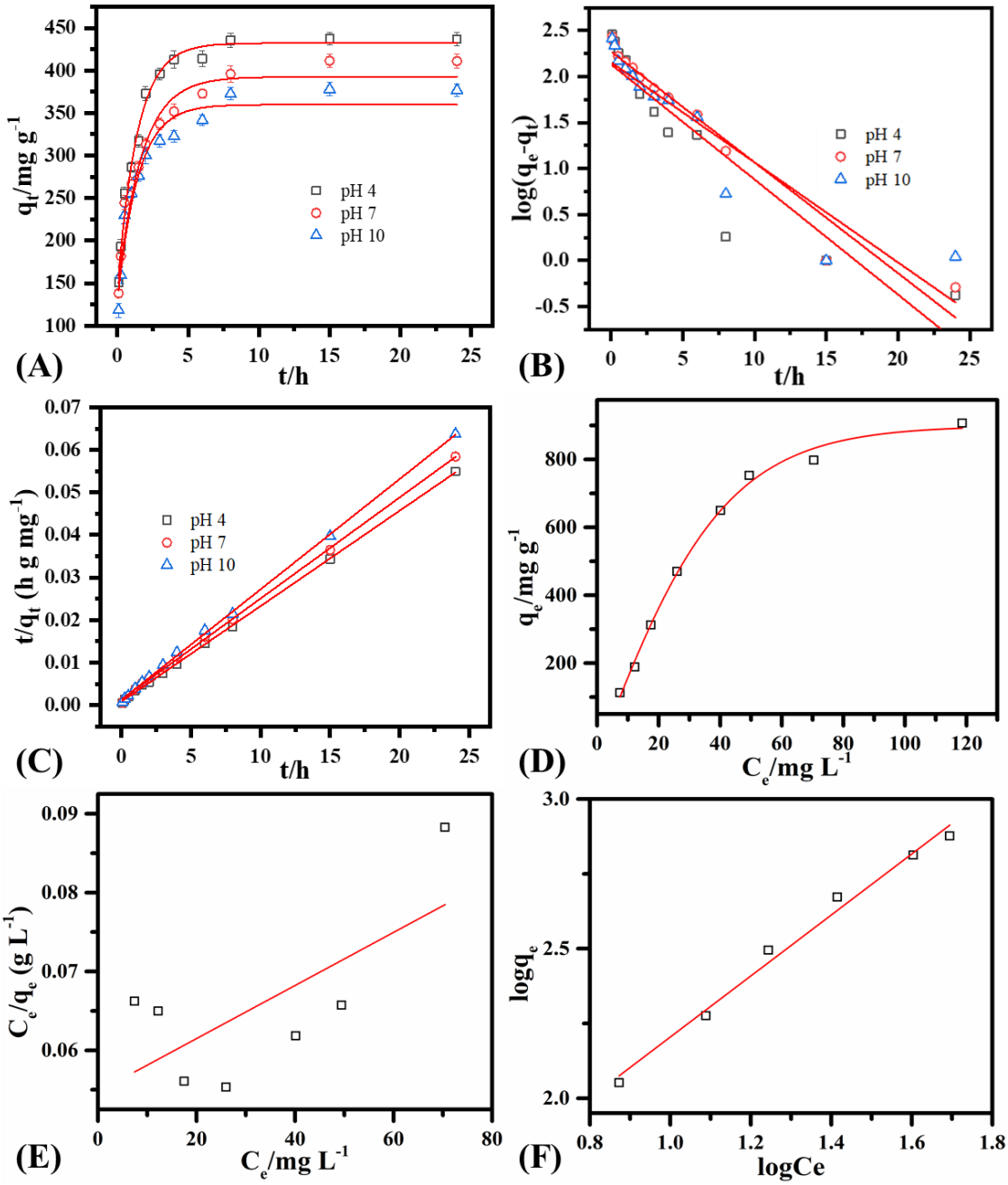

Figure 5. (A) Adsorption kinetic when volume = 100 mL, MgO = 10.0 mg, temperature = 30 °C, shaking speed = 180 rpm, and methyl orange = 50 mg L^{-1}, (B) Pseudo first order, (C) Pseudo second order, (D) Adsorption isotherm when volume = 25 mL, MgO = 5.0 mg, temperature = 30 °C, shaking speed = 180 rpm, pH = 7, and methyl orange 30 - 300 mg L^{-1}. (E) Langmuir isotherm model, (F) Freundlich isotherm model.

Table 2 Adsorption isotherm fitting parameters for methyl orange.

Initial pH	Langmuir isotherm model				Freundlich isotherm model		
	q_{max}/mg g^{-1}	K_L (L mg^{-1})	R_L	R^2	K_F (mg g^{-1}) (L $mg^{-1})^{1/n}$	1/n	R^2
7	2969.24	0.01	0.49	0.38	3.22	1.01	0.99

Table 3 Comparison of different adsorbents in removal capacity for methyl orange

Materials	Removal capacity/mg g^{-1}	Refs.
MgO	940.14	This work
MgO	370.00	[27]
MgO@C	101.80	[28]
MgAl LDHs	443.50	[29]
LDHs membrane	702.83	[30]
Bentonite	156.30	[31]
Polyaniline	75.90	[32]
Carbon nanotubes	310.20	[33]
CuO	121.95	[34]

Adsorption of methylene blue

Figure 6A shows the adsorption kinetic for methylene blue by flower-like MgO microspheres at different initial pH values of the solution. The equilibrium adsorption capacity arrives at 242.91, 252.47, and 306.90 mg g^{-1} for pH 4, 7 and 10 with a short equilibrium time of 1 h, respectively. The adsorption capacity increases with the rise of initial solution pH value under the same investigated conditions. Fig. 6B and C show the linear fitting of the kinetic for pseudo first order and pseudo second order. The obtained results demonstrate that the pseudo-second-order better following the methylene blue adsorption compared with the first-order based on the correlation coefficient values (Table 4). The pseudo-second-order applicability suggests both physical and chemical adsorption of methylene blue on MgO.

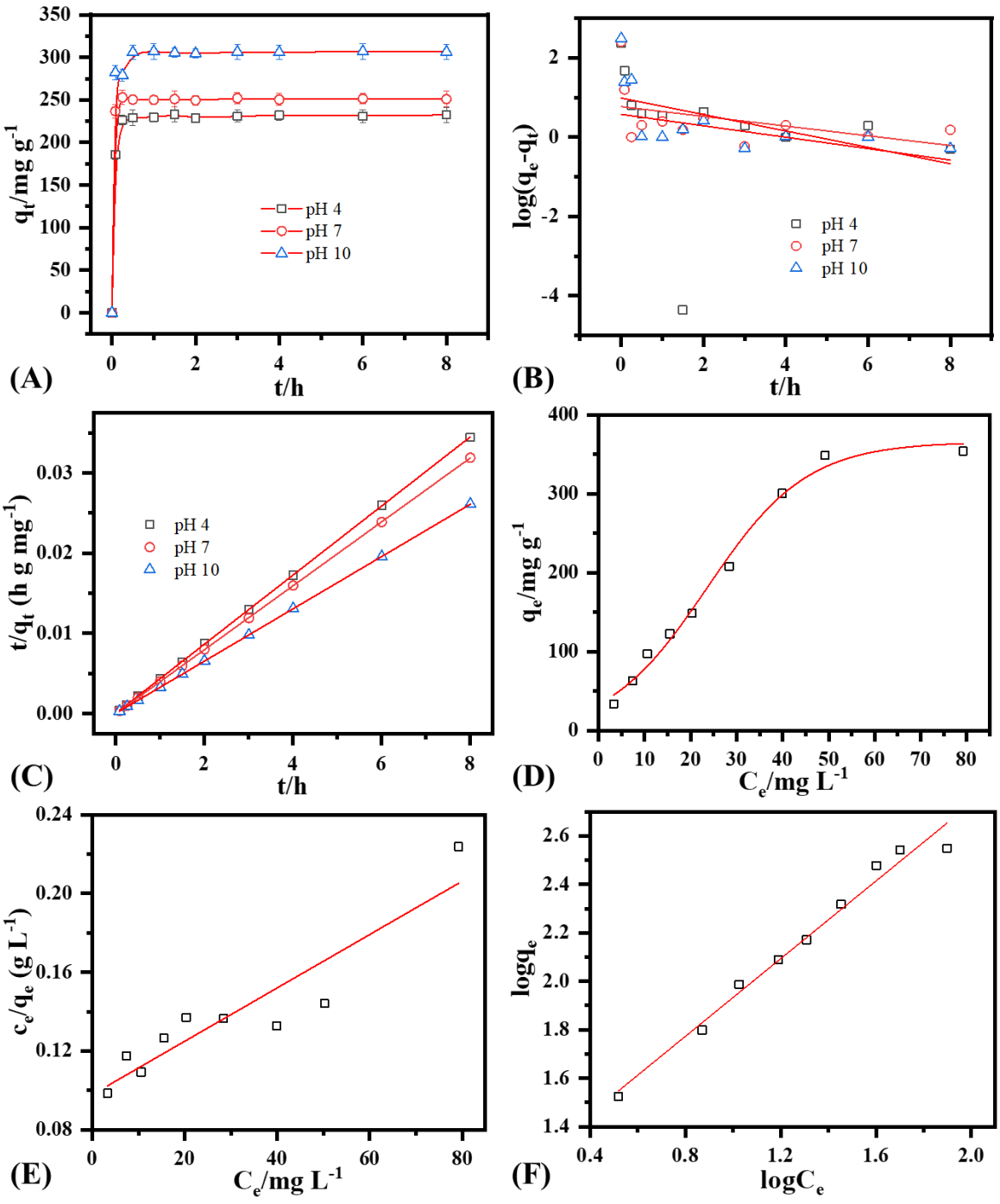

Figure 6. (A) Adsorption kinetic at different solution pH, when volume = 100 mL, MgO = 10.0 mg, temperature = 30 °C, shaking speed = 180 rpm, and methylene blue = 50 mg L^{-1}, (B) Pseudo first-order kinetics (C) Pseudo second-order kinetic (D) Adsorption isotherm when volume = 25 mL, MgO = 5.0 mg, temperature = 30 °C, shaking speed = 180 rpm, pH = 7, and methylene blue 10 mg L^{-1} - 150 mg L^{-1}. (E) Langmuir isotherm model, (F) Freundlich isotherm model.

Figure 6D depicts the adsorption isotherm for methylene blue at the neutral pH. The attained isotherm data are fitted linearly for Langmuir (Fig. 6E) and Freundlich isotherm model (6F). The methylene blue adsorption is better fitted with the Freundlich isotherm model compared with the Langmuir isotherm model based on separation factor and correlation coefficient values as shown in Table 5. The value of separation factor R_L between 0-1 shows the favorable adsorption of methylene blue onto the MgO surface. The maximum capacity for methylene blue is 354.00 mg g^{-1}, which is much higher than those reported in the recent literature for methylene blue as listed in Table 6.

Table 4 Kinetic fitting parameters for methylene blue.

Initial pH	**$q_{e,exp}$/mg g^{-1}**	**Pseudo first order**			**Pseudo second order**		
		$q_{e,cal}$/mg g^{-1}	**k_1**	**R^2**	**$q_{e,cal}$/mg g^{-1}**	**k_2**	**R^2**
4	232.91	1.56	0.14	0.06	232.56	0.32	0.99
7	251.89	2.09	0.12	0.11	251.26	0.85	0.99
10	306.90	2.68	0.21	0.31	306.75	0.35	0.99

Table 5 Isotherm fitting parameters for methylene blue.

Initial pH	**Langmuir isotherm model**				**Freundlich isotherm model**		
	q_{max}/mg g^{-1}	**K_L(L mg^{-1})**	**R_L**	**R^2**	**K_F(mg g^{-1}) (L $mg^{-1})^{1/n}$**	**1/n**	**R^2**
7	740.74	0.01	0.47	0.83	0.125	0.80	0.98

Table 6 Comparison of different adsorbents in removal capacity for methylene blue.

Materials	Removal capacity/mg g^{-1}	Refs.
MgO	354.00	This work
RCE@GO	68.00	[35]
Biochar	241.99	[26]
Fe-Mn binary oxide	72.32	[36]
Lignin	83.20	[37]
Kaolin	52.76	[38]
Th-Py copolymer	250.00	[10]
Carbon composite	138.10	[39]
Metal-organic framework	149.00	[40]

Effect of pH and surface charge

Figure 7A shows the effect of initial dye solution pH on the removal capacity under the investigated conditions. The removal capacity of MO goes down with the increase in solution pH related to the less positive charge on the MgO surface at high pH. On the other hand, the removal capacity of methylene blue goes increase with solution pH related to the more positive charge on MgO at high pH and relatively repulsion between similar charges. This difference in adsorption ability for each dye is related to the nature of the pollutant, and surface charge on MgO [24, 41].

The surface charge plays a key role in the adsorption process when the adsorption occurs because of the electrostatic forces. Figure 7B presents the point of zero charges for MgO, which is 10.38. One can say, the surface of MgO is positively charged, when the solution pH is below the point of zero charges, neutral at point zero charge and negatively charged beyond zero-point charge as shown in Fig. 7C [42-43]. Obviously, the MgO in aqueous solution absorbs a proton from water to form $MgOH_2^+$ based on pH [44-45]. This difference in the adsorption ability for each dye under the similar investigated conditions is related to the surface charge on the MgO [22]. The methyl orange adsorption follows the pseudo-second-order while methylene blue follows the first order with the big difference in the adsorption ability under a similar investigated environment, which mainly results from the nature of two dyes: anionic methylene orange and cationic methylene blue.

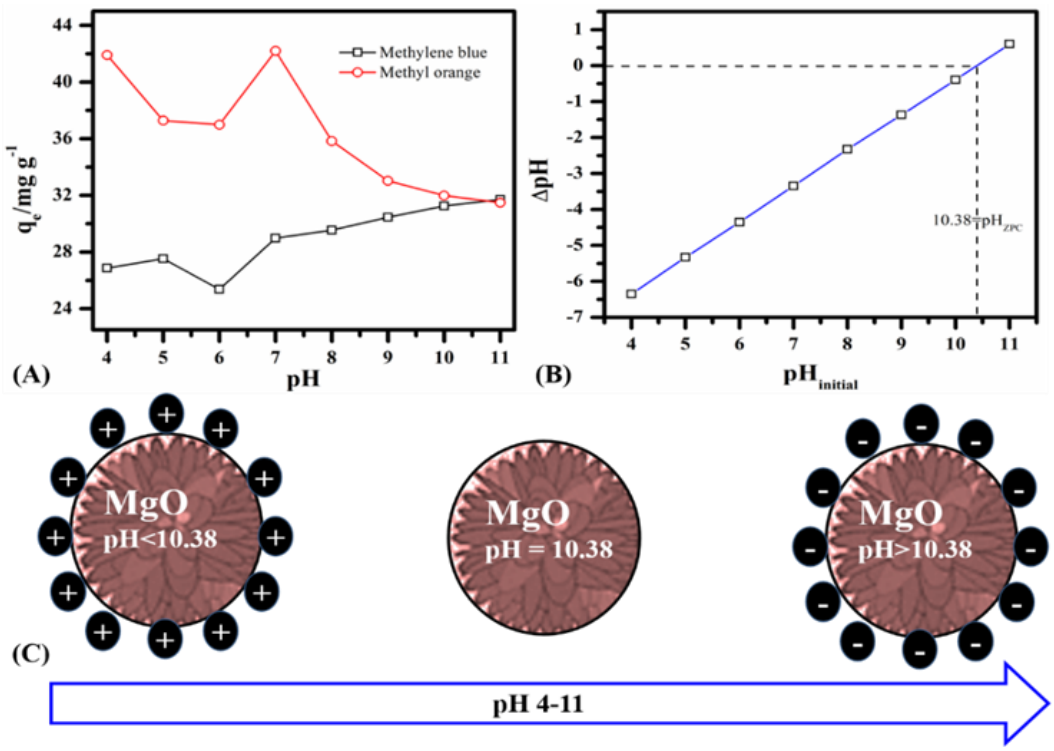

Figure 7. (A) Effect of initial dye solution pH on the removal capacity of methyl orange and methyl blue, (B) Zero-point charge, (C) Surface charge distribution on MgO.

Removal mechanism

In order to investigate the adsorption mechanism for methyl orange and methylene blue, XRD and FT-IR were investigated after adsorption. Fig. 8A presents the XRD of MgO after adsorption of methyl orange and methylene blue. All the peaks belong to magnesium hydroxide as marked in the graph which indicates that the MgO, when added to the aqueous solution of dyes, which changes into magnesium hydroxide reactive species by absorbing a proton from water [11].

Fig. 8B presents the FT-IR spectra of MgO after adsorption in which several new peaks like 1035 cm^{-1} for sulfate along with MgO peaks (3700 cm^{-1} for Mg-O) suggest the successful incorporation of methyl orange into the macroporous MgO microspheres. There is a positive charge on MgO in an aqueous solution that interacts with the different functional groups of methyl orange by electrostatic interaction and hydrogen bonding based on the pH of dyes solution [46-47]. Fig. 8C presents the FT-IR spectra of MgO after adsorption of methylene blue and new peaks at 1640 cm^{-1}, 2361 cm^{-1}, and 3435 cm^{-1} belong to the different functional groups of methylene blue along with MgO peaks, which suggest the successful adsorption of methylene blue. The possible

modes of methylene blue with MgO binding are electrostatic interactions [22, 48]. Although, the adsorption performance of methylene blue is lower compared with methyl orange related to the different nature of dyes along with different binding sites.

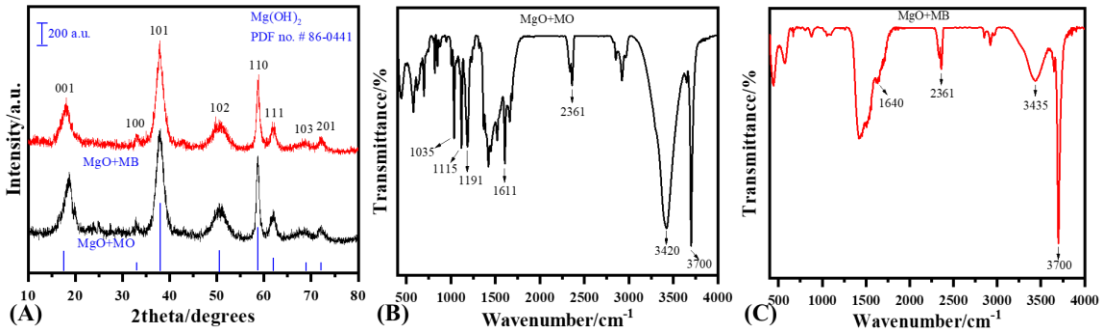

Fig. 8 (A) X-ray diffraction pattern after adsorption of methyl orange and methylene blue, (B) FT-IR spectrum of MgO after adsorption of methyl orange, (C) FT-IR spectrum of MgO after adsorption of methylene blue.

Conclusion

In this work, we monitored the formation process of the macroporous flower-like MgO microspheres in an EG assisted route and understood the difference of adsorption behavior for methyl orange and methylene blue following the initial pH values. The anionic methyl orange and cationic methylene blue adsorption follow the pseudo-second-order with the maximum removal capacity of 940.14 mg g^{-1} and 354.00 mg g^{-1}, respectively. The adsorption ability and rate of MgO for each dye strongly depend upon the surface charge and the charge properties of the dye. This work provides an insight to understand and improve the removal capacity of the adsorbents towards the target pollutant based on their nature.

Acknowledgement

This work is supported by the National Key R & D Program of China (No. 2016YFB0301600), the National Natural Science Foundation of China, the Fundamental Research Funds for the Central Universities (JD1716, 12060093063), and Program for Changjiang Scholars and Innovative Research Team in University (No. IRT1205). S. Ahmed specially thanks the financial support from Chinese Scholarship Council.

References

[1] Koren, Z. C., Modern Chemistry of the Ancient Chemical Processing of Organic Dyes and Pigments. In *Chemical Technology in Antiquity*, Am. Chem. Soc. 2015; Vol. 1211, pp 197-217.
[2] Šuleková, M.; Smrčová, M.; Hudák, A.; Hezelova, M.; Fedorová, M., Organic Colouring Agents in the Pharmaceutical Industry. *Folia Veterinaria* **2017,** *61* (3), 32-46.
[3] Rane, N. R.; Chandanshive, V. V.; Khandare, R. V.; Gholave, A. R.; Yadav, S. R.; Govindwar, S. P., Green remediation of textile dyes containing wastewater by Ipomoea hederifolia L. *RSC Adv.* **2014,** *4* (69), 36623-36632.
[4] Hu, X.-S.; Liang, R.; Sun, G., Super-adsorbent hydrogel for removal of methylene blue dye from aqueous solution. *J. Mater. Chem. A* **2018,** *6* (36), 17612-17624.
[5] Pokharia, A.; Singh, S., *Toxicological Effect of Textile Dyes and their Metabolites: A Review Current Trends in Biotechnology and Chemical Research*. 2015; Vol. 5, p 11-17.
[6] Wang, P.; Tang, Y.; Liu, Y.; Wang, T.; Wu, P.; Lu, X.-Y., Halloysite nanotube@carbon with rich carboxyl groups as a multifunctional adsorbent for the efficient removal of cationic Pb(ii), anionic Cr(vi) and methylene blue (MB). *Environ. Sci.: Nano* **2018,** *5* (10), 2257-2268.
[7] Xu, C.; Shi, S.; Dong, Q.; Zhu, S.; Wang, Y.; Zhou, H.; Wang, X.; Zhu, L.; Zhang, G.; Xu, D., Citric-acid-assisted sol-gel synthesis of mesoporous silicon-magnesium oxide ceramic fibers and their adsorption characteristics. *Ceram. Int.* **2020**. DOI: 10.1016/j.ceramint.2019.12.279
[8] Karimifard, S.; Alavi Moghaddam, M. R., Application of response surface methodology in physicochemical removal of dyes from wastewater: A critical review. *Sci. Total Environ.* **2018,** *640-641*, 772-797.
[9] Momina; Shahadat, M.; Isamil, S., Regeneration performance of clay-based adsorbents for the removal of industrial dyes: a review. *RSC Adv.* **2018,** *8* (43), 24571-24587.
[10] Mishra, A. K.; Shahi, V. K.; Agrawal, N. R.; Das, I., Synthesis, Characterization, and Application of a Thiophene–Pyrrole Copolymer As an Efficient Adsorbent for Removal of Methylene Blue. *J. Chem. Eng. Data* **2018,** *63* (9), 3206-3214.
[11] Ahmed, S.; Pan, J.; Ashiq, M. N.; Li, D.; Tang, P.; Feng, Y., Ethylene glycol-assisted fabrication and superb adsorption capacity of hierarchical porous flower-like magnesium oxide microspheres for phosphate. *Inorg. Chem. Front.* **2019,** *6* (8), 1952-1961.
[12] Ahmed, S.; Guo, Y.; Huang, R.; Li, D.; Tang, P.; Feng, Y., Hexamethylene tetramine-assisted hydrothermal synthesis of porous magnesium oxide for high-efficiency removal of phosphate in aqueous solution. *J. Environ. Chem. Eng.* **2017,** *5* (5), 4649-4655.
[13] Ahmed, S.; Ashiq, M. N.; Li, D.; Tang, P.; Feng, Y., Carbon fiber paper@MgO films: in situ fabrication and high-performance removal capacity for phosphate anions. *Environ. Sci. Pollut. Res.* **2018,** *25* (34), 34788-34792.
[14] Ahmed, S.; Guo, Y.; Li, D.; Tang, P.; Feng, Y., Superb removal capacity of hierarchically porous magnesium oxide for phosphate and methyl orange. *Environ. Sci. Pollut. Res.* **2018,** *25* (25), 24907-24916.
[15] Srivastava, V.; Sharma, Y. C.; Sillanpaa, M., Green synthesis of magnesium oxide nanoflower and its application for the removal of divalent metallic species from synthetic wastewater. *Ceram. Int.* **2015,** *41* (5), 6702-6709.
[16] Zhao, H.; Guo, X.; He, S.; Zeng, X.; Zhou, X.; Zhang, C.; Hu, J.; Wu, X.; Xing, Z.; Chu, L.; He, Y.; Chen, Q., Complex self-assembly of pyrimido[4,5-d]pyrimidine nucleoside supramolecular structures. *Nat. Commun.* **2014,** *5*, 3108.
[17] Min, C.; Yueguang, Z.; Lidan, X.; Youhao, L.; Yongcai, Q.; Shihe, Y.; Weishan, L., Morphology-Conserved Transformations of Metal-Based Precursors to Hierarchically Porous Micro-/Nanostructures for Electrochemical Energy Conversion and Storage. *Adv. Mater.* **2017,** *29* (48), 1607015.
[18] Ruiz-Torres, C. A.; Araujo-Martínez, R. F.; Martínez-Castañón, G. A.; Morales-Sánchez, J. E.; Guajardo-Pacheco, J. M.; González-Hernández, J.; Lee, T.-J.; Shin, H.-S.; Hwang, Y.; Ruiz, F., Preparation of

air stable nanoscale zero valent iron functionalized by ethylene glycol without inert condition. *Chem. Eng. J.* **2018,** *336*, 112-122.
[19] Yang, S.; Huang, P.; Peng, L.; Cao, C.; Zhu, Y.; Wei, F.; Sun, Y.; Song, W., Hierarchical flowerlike magnesium oxide hollow spheres with extremely high surface area for adsorption and catalysis. *J. Mater. Chem. A* **2016,** *4* (2), 400-406.
[20] Kumar, A.; Khan, M.; Fang, L.; Lo, I. M. C., Visible-light-driven N-TiO2@SiO2@Fe3O4 magnetic nanophotocatalysts: Synthesis, characterization, and photocatalytic degradation of PPCPs. *J. Hazard. Mater.* **2019,** *370*, 108-116.
[21] Sing, K. S. W., Reporting physisorption data for gas/solid systems with special reference to the determination of surface area and porosity. *Pur. Appl. Chem.* **1985,** *57*, 603-619.
[22] Huang, R.; He, L.; Zhang, T.; Li, D.; Tang, P.; Zhao, Y.; Feng, Y., Fabrication and Adsorption Behavior of Magnesium Silicate Hydrate Nanoparticles towards Methylene Blue. *Nanomaterials,* **2018,** *8* (5), 271.
[23] Huang, R.; He, L.; Zhang, T.; Li, D.; Tang, P.; Feng, Y., Novel Carbon Paper@Magnesium Silicate Composite Porous Films: Design, Fabrication, and Adsorption Behavior for Heavy Metal Ions in Aqueous Solution. *ACS Appl. Mater. Interfaces* **2018,** *10* (26), 22776-22785.
[24] Huang, R.; Wu, M.; Zhang, T.; Li, D.; Tang, P.; Feng, Y., Template-free Synthesis of Large-Pore-Size Porous Magnesium Silicate Hierarchical Nanostructures for High-Efficiency Removal of Heavy Metal Ions. *ACS Sustainable Chem. Eng.* **2017,** *5* (3), 2774-2780.
[25] Zhong, S.; Sha, H.; He, Y.; Song, G., Hydrothermal synthesis of easy-recycled tobermorite/SiO2/Fe3O4 composites for efficient treatment of phosphorus in wastewater. *Desalin. Water Treat.* **2014,** *52* (22-24), 4305-4313.
[26] Zhu, Y.; Yi, B.; Yuan, Q.; Wu, Y.; Wang, M.; Yan, S., Removal of methylene blue from aqueous solution by cattle manure-derived low temperature biochar. *RSC Adv.* **2018,** *8* (36), 19917-19929.
[27] Li, X.; Xiao, W.; He, G.; Zheng, W.; Yu, N.; Tan, M., Pore size and surface area control of MgO nanostructures using a surfactant-templated hydrothermal process: High adsorption capability to azo dyes. *Colloid. Surfac. A: Physicochem. Eng.* **2012,** *408*, 79-86.
[28] Zheng, X.; Huang, M.; You, Y.; Fu, X.; Liu, Y.; Wen, J., One-pot synthesis of sandwich-like MgO@Carbon with enhanced sorption capacity of organic dye. *Chem. Eng. J.* **2018,** *334*, 1399-1409.
[29] Yao, W.; Yu, S.; Wang, J.; Zou, Y.; Lu, S.; Ai, Y.; Alharbi, N. S.; Alsaedi, A.; Hayat, T.; Wang, X., Enhanced removal of methyl orange on calcined glycerol-modified nanocrystallined Mg/Al layered double hydroxides. *Chem. Eng. J.* **2017,** *307*, 476-486.
[30] Lv, W.; Mei, Q.; Fu, H.; Xiao, J.; Du, M.; Zheng, Q., A general strategy for the synthesis of layered double hydroxide nanoscrolls on arbitrary substrates: its formation and multifunction. *J. Mater. Chem. A* **2017,** *5* (36), 19079-19090.
[31] Chen, Y.; Peng, J.; Xiao, H.; Peng, H.; Bu, L.; Pan, Z.; He, Y.; Chen, F.; Wang, X.; Li, S., Adsorption behavior of hydrotalcite-like modified bentonite for Pb2+, Cu2+and methyl orange removal from water. *Appl. Surf. Sci.* **2017,** *420*, 773-781.
[32] Karri, R. R.; Tanzifi, M.; Tavakkoli Yaraki, M.; Sahu, J. N., Optimization and modeling of methyl orange adsorption onto polyaniline nano-adsorbent through response surface methodology and differential evolution embedded neural network. *J. Environ. Manag.* **2018,** *223*, 517-529.
[33] Ibrahim, R. K.; El-Shafie, A.; Hin, L. S.; Mohd, N. S. B.; Aljumaily, M. M.; Ibraim, S.; AlSaadi, M. A., A clean approach for functionalized carbon nanotubes by deep eutectic solvents and their performance in the adsorption of methyl orange from aqueous solution. *J. Environ. Manag.* **2019,** *235*, 521-534.
[34] Darwish, A. A. A.; Rashad, M.; Al-Aoh, H. A., Methyl orange adsorption comparison on nanoparticles: Isotherm, kinetics, and thermodynamic studies. *Dye. Pigm.* **2019,** *160*, 563-571.
[35] Ren, F.; Li, Z.; Tan, W.-Z.; Liu, X.-H.; Sun, Z.-F.; Ren, P.-G.; Yan, D.-X., Facile preparation of 3D regenerated cellulose/graphene oxide composite aerogel with high-efficiency adsorption towards methylene blue. *J. Colloid Interfac. Sci.* **2018,** *532*, 58-67.

[36] Wang, B.; Zhai, Y.; Wang, T.; Li, S.; Peng, C.; Wang, Z.; Li, C.; Xu, B., Fabrication of bean dreg-derived carbon with high adsorption for methylene blue: Effect of hydrothermal pretreatment and pyrolysis process. *Bioresourc. Technol.* **2019,** *274*, 525-532.
[37] Jin, Y.; Zeng, C.; Lü, Q.-F.; Yu, Y., Efficient adsorption of methylene blue and lead ions in aqueous solutions by 5-sulfosalicylic acid modified lignin. *Int. J. Biol. Macromol.* **2019,** *123*, 50-58.
[38] Mouni, L.; Belkhiri, L.; Bollinger, J.-C.; Bouzaza, A.; Assadi, A.; Tirri, A.; Dahmoune, F.; Madani, K.; Remini, H., Removal of Methylene Blue from aqueous solutions by adsorption on Kaolin: Kinetic and equilibrium studies. *Appl. Clay Sci.* **2018,** *153*, 38-45.
[39] Tong, D. S.; Wu, C. W.; Adebajo, M. O.; Jin, G. C.; Yu, W. H.; Ji, S. F.; Zhou, C. H., Adsorption of methylene blue from aqueous solution onto porous cellulose-derived carbon/montmorillonite nanocomposites. *Appl. Clay Sci.* **2018,** *161*, 256-264.
[40] Zhou, Y.; Qin, L.; Wu, M.-K.; Han, L., A Bifunctional Anionic Metal–Organic Framework: Reversible Photochromism and Selective Adsorption of Methylene Blue. *Cryst. Growth Des.* **2018,** *18* (10), 5738-5744.
[41] Ma, G.; Salahub, S.; Montemagno, C.; Abraham, S., Highly active magnesium oxide nano materials for the removal of arsenates and phosphates from aqueous solutions. *Nano-Structures & Nano-Objects* **2018,** *13*, 74-81.
[42] Ai, L.; Zhang, C.; Meng, L., Adsorption of Methyl Orange from Aqueous Solution on Hydrothermal Synthesized Mg–Al Layered Double Hydroxide. *J. Chem. Eng. Data* **2011,** *56* (11), 4217-4225.
[43] Yu, Y.; Paul Chen, J., Key factors for optimum performance in phosphate removal from contaminated water by a Fe–Mg–La tri-metal composite sorbent. *J. Colloid Interfac. Sci.* **2015,** *445*, 303-311.
[44] Tripathi, S.; Bose, R.; Roy, A.; Nair, S.; Ravishankar, N., Synthesis of Hollow Nanotubes of Zn2SiO4 or SiO2: Mechanistic Understanding and Uranium Adsorption Behavior. *ACS Appl. Mater. Interfaces* **2015,** *7* (48), 26430-26436.
[45] Salem, A.-N. M.; Ahmed, M. A.; El-Shahat, M. F., Selective adsorption of amaranth dye on Fe3O4/MgO nanoparticles. *J. Mol. Liq.* **2016,** *219*, 780-788.
[46] Wong, S.; Tumari, H. H.; Ngadi, N.; Mohamed, N. B.; Hassan, O.; Mat, R.; Saidina Amin, N. A., Adsorption of anionic dyes on spent tea leaves modified with polyethyleneimine (PEI-STL). *J. Clean. Prod.* **2019,** *206*, 394-406.
[47] Chen, H.; Zhong, A.; Wu, J.; Zhao, J.; Yan, H., Adsorption Behaviors and Mechanisms of Methyl Orange on Heat-Treated Palygorskite Clays. *Ind. Eng. Chem. Res.* **2012,** *51* (43), 14026-14036.
[48] He, K.; Zeng, G.; Chen, A.; Huang, Z.; Peng, M.; Huang, T.; Chen, G., Graphene hybridized polydopamine-kaolin composite as effective adsorbent for methylene blue removal. *Comp. B: Eng.* **2019,** *161*, 141-149.